CCC 2008 - Challenges for Civil Construction
Torres Marques et al. (Eds)

MULTI-FIXED SMEARED 3D CRACK MODEL TO SIMULATE THE BEHAVIOR OF FIBER REINFORCED CONCRETE STRUCTURES

A. Ventura-Gouveia[*], Joaquim Barros[†], Álvaro Azevedo[+] and J. Sena-Cruz[†]

[*]DEC, ISISE, School of Technology, Polytechnic Institute of Viseu
Campus de Repeses, 3504-510 Viseu, Portugal
e-mail: ventura@dcivil.estv.ipv.pt
web page: http://www.dcivil.estv.ipv.pt/dep/dcivil

[†]DEC, ISISE, School of Engineering, University of Minho
Campus de Azurem, 4800-058 Guimarães, Portugal
e-mail: barros@civil.uminho.pt, jsena@civil.uminho.pt
web page: http://www.civil.uminho.pt/composites

[+]Faculty of Engineering of the University of Porto (FEUP)
University of Porto
Rua Dr. Roberto Frias, s/n, 4200-465 Porto, Portugal
e-mail: alvaro@fe.up.pt, web page: http://www.fe.up.pt/~alvaro

Keywords: Smeared 3D Crack Model, Punching, Shear Softening Diagram, Material Nonlinear Analysis, Finite Element Method.

Summary: *When a concrete structure is subjected to a multi-stress state, different crack modes can be developed. To simulate with enough accuracy these fracture modes, a three-dimensional model must be used. In the present work, a multi-fixed smeared 3D crack model is proposed to predict the normal and shear failure modes of concrete structures. Softening stress-strain diagrams are proposed to model, after crack initiation, the normal and shear components. The performance of the developed model was appraised by simulating the behavior observed in punching tests with lightweight panels of steel fiber reinforced self-compacting concrete (SFRSCC).*

1 INTRODUCTION

Smeared and discrete crack concepts can be used to model the crack propagation in concrete structures [1]. Since fiber reinforcement can assure the formation of diffuse crack patterns, a smeared crack model can be conceptually more appropriate, and more effective from the computational point-of-view, for the simulation of the behavior of fiber reinforced concrete structures. Previous research indicated that fracture mode I can be simulated using a tri-linear softening diagram, whose parameters can be obtained from direct tensile tests or performing inverse analysis with the force-deflection data registered in three-point notched beam bending tests carried out according to the RILEM TC 162-TDF recommendations [2]. To simulate the shear fracture modes, a shear retention factor is currently used. With this model the shear stress transfer between the crack planes decreases with the increase of the normal crack strain, according to an assumed relation. In most structures assumed as behaving in plane stress state, this strategy provides simulations with reasonable accuracy. Exceptions occur in structures which fail by the formation of a critical shear crack. For these cases, the simulation of the structural softening with high accuracy requires the adoption of a softening crack shear stress *vs.* crack shear strain relationship. This procedure introduces some difficulties in the convergence of the incremental-iterative procedure of the standard Newton-Raphson method adopted for the structural nonlinear analysis. However, even with these strain-softening crack

constitutive laws, adopted to simulate the in-plane fracture modes, punching rupture cannot be accurately simulated in laminate structures submitted to concentrated loads. Using the Reissner-Mindlin theory for shell structures, the structural softening registered in the punching tests with lightweight steel fiber reinforced self-compacting concrete (SFRSCC) is well predicted when a strain-softening diagram to simulate both out-of-plane shear components is adopted [3]. This model, however, cannot reproduce the crack pattern observed in these punching tests, since the cracks are assumed to be orthogonal to the middle surface of the shell. To simulate this type of failure, a full 3D crack constitutive model is required [4].

In the present work, a multi-fixed smeared 3D crack model, under the framework of the finite element method, is proposed to simulate the behavior of fiber reinforced concrete structures failing in shear. The model was included in the 3D solid element of the FEMIX computer code, which is a general purpose finite element program [5].

The proposed model is described and its performance is appraised by simulating punching tests with lightweight panels of steel fiber reinforced self-compacting concrete (SFRSCC) [6].

2 NUMERICAL MODEL

2.1 Introduction

In a previous work [3], the Reissner-Mindlin theory was adopted in the prediction of the shear failure of layered shell structures. The material nonlinear behavior was simulated by considering the crack propagation in the layers that discretize a finite element. After crack formation, the crack constitutive laws and the out-of-plane shear stress-strain relationships were modeled by softening diagrams. Modeling the softening of both out-of-plane shear components was decisive to accurately simulate the failure mode registered in the punching tests. However, since the model predicts cracks that are orthogonal to the middle surface of the shell, the punching failure surface cannot be obtained. To simulate this complex failure mode a three-dimensional approach must be used. In the present work the multi-fixed smeared 2D crack model, previously implemented in the FEMIX computer code [7], is generalized to a multi-fixed smeared 3D crack model (implemented with solid finite elements). The fracture mode I is simulated with a tri-linear stress-strain diagram. The characterization of the shear fracture modes is much more complex, since the shear stress transfer between the crack surfaces depends on several parameters, such as concrete lateral confinement, crack opening, roughness of the crack surfaces, concrete strength class, number of cracks and its relative orientation, etc. A softening shear stress-strain diagram is proposed to simulate the shear stress transfer between the crack surfaces.

2.2. Formulation

When the material behavior is considered to be nonlinear, its constitutive matrix depends on the stress or strain levels. In this case, to obtain the solution of the resulting system of nonlinear equations, an incremental-iterative technique is normally used. In this procedure the external load is applied incrementally and the relationship between incremental strain and stress is given by the following equation

$$\Delta\underline{\sigma} = \underline{D}\ \Delta\underline{\varepsilon} \tag{1}$$

where $\Delta\underline{\sigma}$ represents the stress increment, $\Delta\underline{\varepsilon}$ is the strain increment and $\underline{D}$ is the tangent constitutive matrix.

In smeared crack models the total incremental strain of the cracked material is decomposed into an incremental strain vector of the crack, $\Delta\underline{\varepsilon}^{cr}$, and an incremental strain vector of the uncracked concrete between the cracks, $\Delta\underline{\varepsilon}^{co}$ [7].

$$\Delta\underline{\varepsilon} = \Delta\underline{\varepsilon}^{co} + \Delta\underline{\varepsilon}^{cr} \tag{2}$$

For the three-dimensional case, the incremental local crack strain vector, $\Delta\underline{\varepsilon}_{\ell}^{cr}$, is defined by

$$\Delta\underline{\varepsilon}_{\ell}^{cr} = \left\{\Delta\varepsilon_n^{cr}, \Delta\gamma_{t_1}^{cr}, \Delta\gamma_{t_2}^{cr}\right\}^T \tag{3}$$

and, in the global coordinate system, by

$$\Delta\underline{\varepsilon}^{cr} = \left\{\Delta\varepsilon_1^{cr}, \Delta\varepsilon_2^{cr}, \Delta\varepsilon_3^{cr}, \Delta\gamma_{23}^{cr}, \Delta\gamma_{31}^{cr}, \Delta\gamma_{12}^{cr}\right\}^T \tag{4}$$

Eq. (5) represents the relation between $\Delta\underline{\varepsilon}_{\ell}^{cr}$ and $\Delta\underline{\varepsilon}^{cr}$

$$\Delta\underline{\varepsilon}^{cr} = \left[\underline{T}^{cr}\right]^T \Delta\underline{\varepsilon}_{\ell}^{cr} \tag{5}$$

where $\underline{T}^{cr}$ is the transformation matrix (see Figure 1)

$$\underline{T}^{cr} = \begin{bmatrix} a_{11}^2 & a_{12}^2 & a_{13}^2 & 2a_{12}a_{13} & 2a_{11}a_{13} & 2a_{11}a_{12} \\ a_{11}a_{21} & a_{12}a_{22} & a_{13}a_{23} & a_{12}a_{23}+a_{13}a_{22} & a_{11}a_{23}+a_{13}a_{21} & a_{11}a_{22}+a_{12}a_{21} \\ a_{11}a_{31} & a_{12}a_{32} & a_{13}a_{33} & a_{13}a_{32}+a_{12}a_{33} & a_{13}a_{31}+a_{11}a_{33} & a_{12}a_{31}+a_{11}a_{32} \end{bmatrix} \tag{6}$$

The components a_{11}, a_{12} and a_{13} form a vector that follows the direction of the n local axis; a_{21}, a_{22} and a_{23} form a vector that defines the t_1 local axis; a_{31}, a_{32} and a_{33} form a vector that defines the t_2 local axis. All these vectors are defined in the global coordinate system.

According to the classical fracture mechanics, and for the case of a plate, three different types of crack modes can be considered. The crack opening mode (mode I); the shearing mode (mode II - in-plane shear) and the tearing fracture mode (mode III - out-of-plane shear). For the case of general solids, the distinction between mode II and mode III can be dropped [8]. For this reason, in the present model mode II and mode III are designated as sliding modes in $\hat{t}_1$ and $\hat{t}_2$ direction, respectively.

The local incremental stress vector, $\Delta\underline{\sigma}_{\ell}^{cr}$, can be defined by

$$\Delta\underline{\sigma}_{\ell}^{cr} = \left\{\Delta\sigma_n^{cr}, \Delta\tau_{t_1}^{cr}, \Delta\tau_{t_2}^{cr}\right\}^T \tag{7}$$

where $\Delta\sigma_n^{cr}$ is the mode I incremental crack normal stress, $\Delta\tau_{t_1}^{cr}$ is the sliding mode incremental crack shear stress in $\hat{t}_1$ direction and $\Delta\tau_{t_2}^{cr}$ is the sliding mode incremental crack shear stress in $\hat{t}_2$ direction.

Figure 1 represents the crack stress components in the local coordinate system of the crack and the corresponding displacements: the opening displacement, w, the sliding displacement in $\hat{t}_1$ direction, s_1, and the sliding displacement in $\hat{t}_2$ direction, s_2.

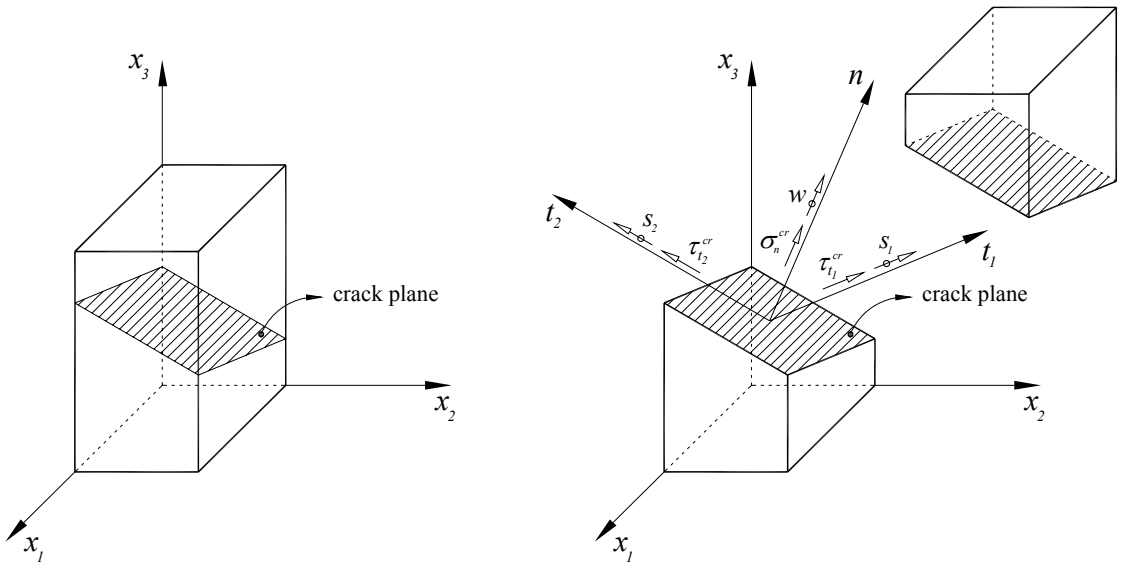

Figure 1. Crack stress components, displacements and local coordinate system of the crack.

In the global coordinate system the incremental stress components are

$$\Delta\underline{\sigma} = \left\{\Delta\sigma_1, \Delta\sigma_2, \Delta\sigma_3, \Delta\tau_{23}, \Delta\tau_{31}, \Delta\tau_{12}\right\}^T \tag{8}$$

The relation between $\Delta\underline{\sigma}$ and $\Delta\underline{\sigma}_{\ell}^{cr}$ is

$$\Delta\underline{\sigma}_{\ell}^{cr} = \underline{T}^{cr}\Delta\underline{\sigma} \tag{9}$$

Assuming a linear elastic behavior for the concrete between cracks, the relation between $\Delta\underline{\varepsilon}^{co}$ and $\Delta\underline{\sigma}$ is given by

$$\Delta\underline{\sigma} = \underline{D}^{co}\Delta\underline{\varepsilon}^{co} \tag{10}$$

with

$$\underline{D}^{co} = \frac{E}{(1+\nu)(1-2\nu)}\begin{bmatrix} (1-\nu) & \nu & \nu & 0 & 0 & 0 \\ \nu & (1-\nu) & \nu & 0 & 0 & 0 \\ \nu & \nu & (1-\nu) & 0 & 0 & 0 \\ 0 & 0 & 0 & \frac{1-2\nu}{2} & 0 & 0 \\ 0 & 0 & 0 & 0 & \frac{1-2\nu}{2} & 0 \\ 0 & 0 & 0 & 0 & 0 & \frac{1-2\nu}{2} \end{bmatrix} \tag{11}$$

being E the Young's modulus and ν the Poisson's ratio of the undamaged concrete.

In the crack zone, the relationship between $\Delta\underline{\varepsilon}_{\ell}^{cr}$ and $\Delta\underline{\sigma}_{\ell}^{cr}$ is given by

$$\Delta\underline{\sigma}_{\ell}^{cr} = \underline{D}^{cr}\,\Delta\underline{\varepsilon}^{cr} \tag{12}$$

where

$$\underline{D}^{cr} = \begin{bmatrix} D_n^{cr} & 0 & 0 \\ 0 & D_{t_1}^{cr} & 0 \\ 0 & 0 & D_{t_2}^{cr} \end{bmatrix} \tag{13}$$

is the crack constitutive matrix.

Combining equations (1)-(13) and using the multi-fixed smeared crack concept [9], the following constitutive law for the cracked concrete can be obtained [7]

$$\Delta\underline{\sigma} = \left(\underline{D}^{co} - \underline{D}^{co}\left[\hat{\underline{T}}^{cr}\right]^{T}\left(\hat{\underline{D}}^{cr} + \hat{\underline{T}}^{cr}\,\underline{D}^{co}\left[\hat{\underline{T}}^{cr}\right]^{T}\right)^{-1}\hat{\underline{T}}^{cr}\,\underline{D}^{co}\right)\Delta\underline{\varepsilon} \tag{14}$$

which is equivalent to

$$\Delta\underline{\sigma} = \underline{D}^{crco}\;\Delta\underline{\varepsilon} \tag{15}$$

where $\underline{D}^{crco}$ is the following constitutive matrix for the cracked concrete

$$\underline{D}^{co} - \underline{D}^{co}\left[\hat{\underline{T}}^{cr}\right]^{T}\left(\hat{\underline{D}}^{cr} + \hat{\underline{T}}^{cr}\,\underline{D}^{co}\left[\hat{\underline{T}}^{cr}\right]^{T}\right)^{-1}\hat{\underline{T}}^{cr}\,\underline{D}^{co} \tag{16}$$

In this equation, $\hat{\underline{D}}^{cr}$ and $\hat{\underline{T}}^{cr}$ take into account the assembly of multi-directional cracks and are defined by

$$\hat{\underline{D}}^{cr} = \begin{bmatrix} \underline{D}_1^{cr} & \underline{0} & \ldots & \underline{0} \\ \underline{0} & \underline{D}_2^{cr} & \ldots & \underline{0} \\ \ldots & \ldots & \ldots & \ldots \\ \underline{0} & \underline{0} & \ldots & \underline{D}_{n_{cr}}^{cr} \end{bmatrix} \tag{17}$$

and

$$\hat{\underline{T}}^{cr} = \left\{ \underline{T}_1^{cr} \quad \underline{T}_2^{cr} \quad \ldots \quad \underline{T}_{n_{cr}}^{cr} \right\}^{T} \tag{18}$$

In equations (17) and (18), D_i^{cr} and $\underline{T}_i^{cr}$ correspond to the crack constitutive matrix and to the crack transformation matrix of the *i*-th crack, respectively.

In Eq. (13), D_n^{cr}, $D_{t_1}^{cr}$ and $D_{t_2}^{cr}$ represent, respectively, the opening fracture mode stiffness modulus, the sliding mode stiffness modulus in the $\hat{t}_1$ direction and the sliding mode stiffness modulus

in the $\hat{t}_2$ direction. The fracture mode I modulus, D_n^{cr}, is defined in Figure 2, where α_i and ξ_i are the parameters that define the shape of the crack normal stress *vs.* crack normal strain diagram ($\alpha_1 = \sigma_{n,2}^{cr} / \sigma_{n,1}^{cr}$, $\alpha_2 = \sigma_{n,3}^{cr} / \sigma_{n,1}^{cr}$, $\xi_1 = \varepsilon_{n,2}^{cr} / \varepsilon_{n,ult}^{cr}$ and $\xi_2 = \varepsilon_{n,3}^{cr} / \varepsilon_{n,ult}^{cr}$). The ultimate crack normal strain, $\varepsilon_{n,u}^{cr}$, depends on the α_i and ξ_i parameters, on the fracture energy, $G_{f,n}$, on the tensile strength, ($f_{ct} = \sigma_{n,1}^{cr}$), and on the crack band width, l_b [7],

$$\varepsilon_{n,u}^{cr} = \frac{2}{\xi_1 + \alpha_1 \xi_2 - \alpha_2 \xi_1 + \alpha_2} \cdot \frac{G_{f,n}}{f_{ct} l_b} \tag{19}$$

The sliding fracture mode modulus, $D_{t_1}^{cr}$ or $D_{t_2}^{cr}$, can be obtained with,

$$D_{t_1}^{cr} = D_{t_2}^{cr} = \frac{\beta}{1-\beta} G_c \tag{20}$$

where G_c is the concrete elastic shear modulus and β is the shear retention factor, defined as a constant value or as a function of the current crack normal strain, ε_n^{cr}, and of the ultimate crack normal strain, $\varepsilon_{n,ult}^{cr}$ (see Eq. (21)). When a linear decrease of β with the increase of ε_n^{cr} is assumed, then $p_1 = 1$. Larger values of the exponent p_1 correspond to a faster decrease of the parameter β [7].

$$\beta = \left(1 - \frac{\varepsilon_n^{cr}}{\varepsilon_{n,ult}^{cr}}\right)^{p_1} \tag{21}$$

To improve the accuracy of the simulation of structures failing in shear, an alternative softening constitutive law [10] was included to model the crack shear stress transfer in $\hat{t}_1$ and $\hat{t}_2$ directions (see Figure 3).

For each crack shear component, the crack peak shear strain is obtained using the crack shear strength, $\tau_{t,p}^{cr}$, and the crack shear modulus obtained from Eq. (20) with a constant shear retention factor.

$$\gamma_{t_1,p}^{cr} = \gamma_{t_2,p}^{cr} = \frac{\tau_{t,p}^{cr}}{D_{t,1}^{cr}} \tag{22}$$

The ultimate crack shear strain in each sliding direction depends on the crack shear strength, $\tau_{t,p}^{cr}$, on the shear fracture energy, $G_{f,s}$, and on the crack band-width, l_b, as follows

$$\gamma_{t_1,u}^{cr} = \gamma_{t_2,u}^{cr} = \frac{2 G_{f,s}}{\tau_p^{cr} \, l_b} \tag{23}$$

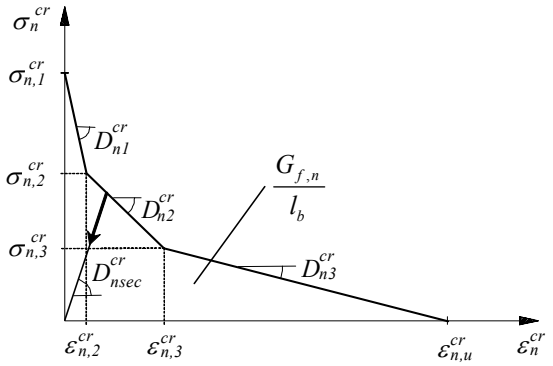

Figure 2. Tri-linear stress-strain diagram.

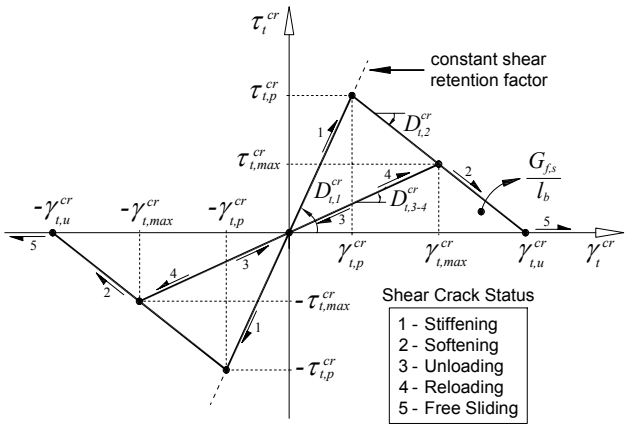

Figure 3. Generic crack shear stress and crack shear strain diagram and the adopted shear crack statuses.

In the present approach it is assumed that the crack band width used for assuring mesh independence when modeling fracture mode I can also be used to define the dissipated energy in the shear fracture process.

A simple Rankine criterion is used to detect crack initiation. When the maximum principal tensile stress exceeds the tensile strength at an integration point (IP) of a finite element, the material contained in its influence volume changes from uncracked to cracked state. The crack surface is considered to be normal to the direction of the maximum principal stress. The crack normal tensile stress follows the softening branches of the tri-linear diagram of Figure 2, thus defining the fracture mode I modulus, D_n^{cr}. When a shear softening diagram is used, the crack shear stresses and the sliding moduli of the fracture modes, $D_{t_1}^{cr}$ and $D_{t_2}^{cr}$, are obtained from the diagram represented in Figure 3. Each sliding mode follows an independent shear softening diagram. The shear softening diagram starts at the origin because, according to the above described criterion, when a crack initiates the shear stress across the crack is zero. As a consequence of the rotation of the principal axes, shear stresses can develop across the surfaces of the crack [10]. The crack shear stress increases linearly until the crack shear strength is reached (first branch of the shear crack diagram), followed by a decrease in shear stress. The second branch (softening branch) is used afterwards to evaluate the shear stress and the sliding fracture modes moduli.

As a consequence of the formation of other cracks in the neighborhood of existing cracks, these existing cracks can close or reopen. The model must take into account this change of crack status. The multi-fixed 2D smeared crack model [7] takes into account these crack status modifications. In the present 3D model a similar approach is used for the opening mode I and for both sliding modes. An eventual coupling between the normal and shear modes was not considered. So a crack can, for example, unload in mode I, soften in sliding mode in $\hat{t}_1$ direction and reload in sliding mode in $\hat{t}_2$ direction. For this reason, the model treats separately the normal crack status, the shear crack status in $\hat{t}_1$ direction and the shear crack status in $\hat{t}_2$ direction. For the sliding modes the shear crack statuses are shown in Figure 3. A secant approach is used for the unloading/reloading behavior, as shown in Figure 2 and Figure 3.

3. MODEL APPRAISAL

The performance of the proposed constitutive model is assessed by simulating the behavior observed in a punching test with a lightweight panel prototype of SFRSCC. The test layout and the test setup are represented in Figure 4. The details about the experimental program can be found elsewhere [6]. The finite element model, the load and the support conditions used in the numerical simulation of the punching test are shown in Figure 5. Only one quarter of the panel is used in the simulation due to double symmetry. Serendipity 20 noded solid elements with 2×2×3 Gauss-Legendre integration scheme are used (3 integration points in the panel orthogonal direction). Three solid elements are used along the thickness of 110 mm, while in the lightweight zone (shaded elements in Figure 5) one solid element is used along the thickness. The dashed line represents the support of the panel.

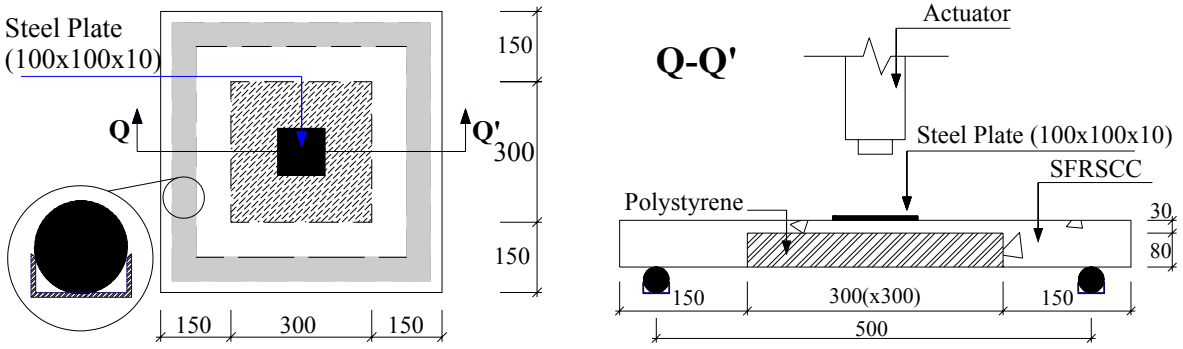

Figure 4. (a) Test panel prototype for the punching resistance and (b) test setup (dimensions in mm).

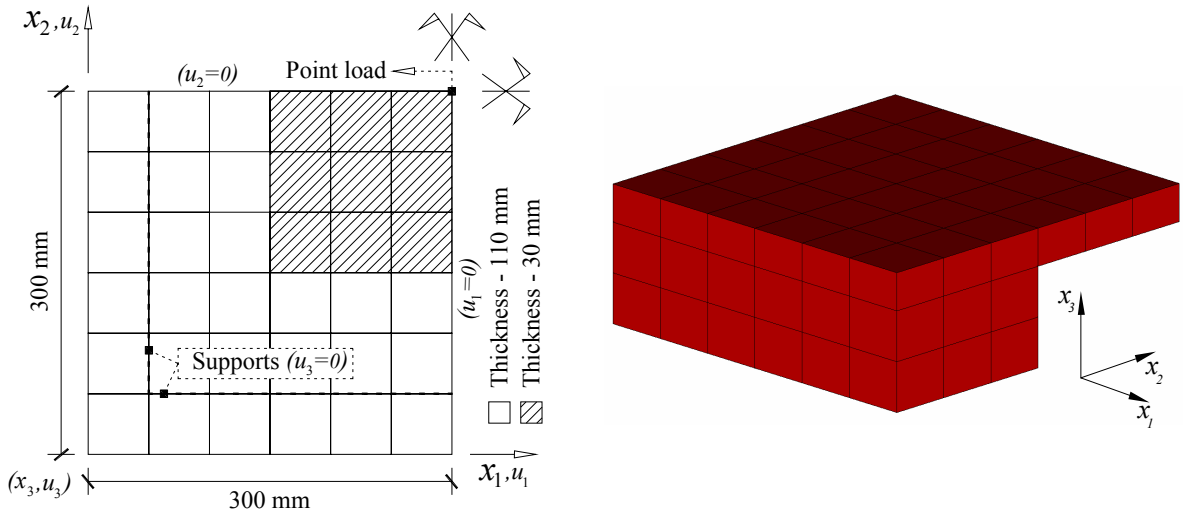

Figure 5. Geometry, mesh, load and support conditions used in the numerical simulation of the punching test.

The values of the parameters of the constitutive model used in the simulation of the punching test are listed in Table 1. Two numerical simulations were carried out. In the former, the shear stress transfer in both sliding modes is simulated according to equations (20) and (21) with p_1=2. In the latter, the crack shear stress *vs.* crack shear strain diagram represented in Figure 3 is used to model both shear sliding modes. In both simulations the values of the parameters to model the fracture mode I were obtained from inverse analysis, whose strategy is described in another publication [11].

Table 1. Values of the parameters of the constitutive model used in the simulation of the punching test.

Poisson's ratio	$\nu = 0.15$
Initial Young's modulus	$E_c = 31000.0 \text{ N/mm}^2$
Compressive strength	$f_c = 52.0 \text{ N/mm}^2$
Tri-linear tension softening diagram of SFRSCC	$f_{ct} = 3.5 \text{ N/mm}^2$; $G_{f,n} = 4.3 \text{ N/mm}$; $\xi_1 = 0.009$; $\alpha_1 = 0.5$; $\xi_2 = 0.15$; $\alpha_2 = 0.59$
Parameter defining the mode I fracture energy available to the new crack	$p_2 = 2$
Softening crack shear stress-strain diagram	$\tau_{t,p}^{cr} = 2.0 \text{ N/mm}^2$; $G_{f,s} = 5.0 \text{ N/mm}$; $\beta = 0.5$
Crack band-width	Cube root of the volume of the integration point
Threshold angle	$\alpha_{th} = 30^o$

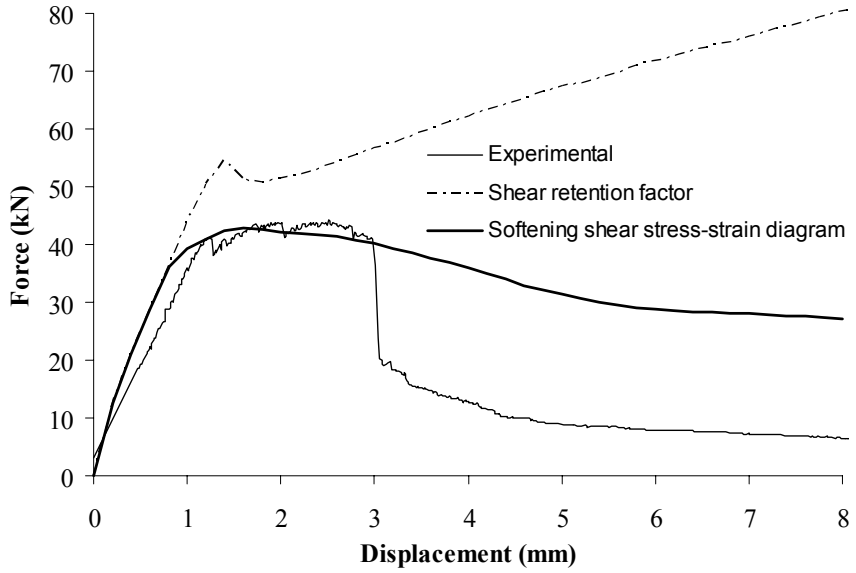

Figure 6. Relationship between the force and the deflection at the center of the test panel.

From Figure 6 it is observed that, in the experimental test, at a deflection of about 1.2 mm of the panel central point, the panel load carrying capacity was almost retained up to a deflection of about 3 mm, after that an abrupt load decay occurred due to the formation of a shear failure surface, typical of a punching rupture. However, using the concept of shear retention factor, the model predicted an increase of the panel load carrying capacity with the increase of the panel deflection. According to this approach, the shear stresses in $\hat{t}_1$ and $\hat{t}_2$ sliding directions ($\tau_{t_1}^{cr}$, $\tau_{t_2}^{cr}$) increase with the increase of the corresponding shear strains ($\gamma_{t_1}^{cr}$, $\gamma_{t_2}^{cr}$). Only after the mode I fracture energy has been exhausted ($\varepsilon_n^{cr} \geq \varepsilon_{n,u}^{cr}$, see Figure 2), both crack shear stress components become null. However, for this type of problem, where the crack shear constitutive components are mandatory, mainly after a certain deflection, the formulation of these components should allow that the shear stress components decrease with the increase of the crack opening, which requires the use of a shear softening diagram, similar to that represented in Figure 3. In fact, the second simulation, which is based on this approach, captured the plateau registered experimentally (see Figure 6), since the parameters of this diagram were evaluated, by back-fitting analysis, in order to reproduce this phase of the panel response, as much as possible. However, the abrupt load decay observed in the experimental test, at a deflection of about 3 mm, was not captured by this second approach, since the numerical simulation predicted a continuous, but smooth, degradation of the panel load carrying capacity. It is verified that a decrease of $G_{f,s}$ causes a decrease on the panel load carrying capacity, mainly in its structural softening phase, and the abrupt load decay is still not captured. It appears that more sophisticated shear crack softening diagrams are necessary for capturing abrupt crack shear stress decays, which is an undergoing research.

4. CONCLUSIONS

In the present work a multi-fixed smeared 3D crack model is proposed. The developed model is based on the finite element method and was implemented in the FEMIX computer code. In an attempt to simulate the shear strain gradient that occurs in punching tests, a shear softening diagram was proposed to determine both crack shear stress components from the corresponding crack shear strains. The crack shear stress transfer can also be simulated using the concept of shear retention factor, which assumes a unitary value at crack initiation and a null value when the mode I fracture energy is exhausted.

The performance of the model is appraised by using the results obtained in a punching test with a lightweight panel prototype of steel fiber reinforced self-compacting concrete.

Two simulations are discussed: one using the concept of shear retention factor and the other using a softening diagram to model both crack shear components. The former simulation cannot reproduce the plateau and the load decay registered in the experimental test, in terms of applied load *vs.* deflection of the panel central point. In fact, the load increases with the increase of the panel deflection. The simulation based on the use of a softening diagram to model the shear crack components captures the panel load carrying capacity, but the load decay registered experimentally, typical of structures failing in punching, is not reproduced numerically. More sophisticated shear softening diagrams are being explored in order to improve the capabilities of the model developed in the context of the present research program.

ACKNOWLEDGMENTS

The first author acknowledges the financial support of FCT, PhD Grant number SFRH/BD/23326/2005. The study reported in this paper is part of the research program PABERPRO – Conception and implementation of production system of lightweight steel fibre reinforced self-compacting concrete panels" supported by Program POCI 2010 – IDEIA, Project

nº 13-05-04-FDR-00007, contract reference ADI/2007/V4.1/0049. This project involves the Companies PREGAIA and CIVITEST, and the University of Minho. The authors wish to acknowledge the materials generously supplied by Bekaert (fibres), SECIL (cement), and Comital (limestone filler).

REFERENCES

[1] de Borst, R.; Remmers, J.J.C.; Needleman, A.; Marie-Angele Abellan, "Discrete vs. smeared crack models for concrete fracture: bridging the gap", *Int. J. Numer. Anal. Meth. Geomech.*, 28:583–607, 2004.

[2] RILEM TC 162-TDF. "Test and design methods for steel fibre reinforced concrete - Final Recommendation." *Materials and Structures 35(253)*, pp. 579-582, 2002.

[3] Ventura-Gouveia, A.; Barros, J.A.O.; Azevedo, A.F.M.; Sena-Cruz, J.M., "Crack Constitutive Model to Simulate the Behavior of Fiber Reinforced Concrete Structures Failing in Punching.", *CMNE/CILAMCE 2007*, Abstract pp. 287, Paper nº 232 published in CD – FEUP, 13 pp., Porto, 13-15 June 2007.

[4] Barzegar, F. and Maddipudi, S., "Three-dimensional modeling of concrete structures. I: Plain Concrete", *Journal of Structural Engineering, 123(10)*, pp. 1339-1346, October 1997.

[5] Sena-Cruz, J.M.; Barros, J.A.O.; Azevedo, A.F.M.; Ventura-Gouveia, A., "Numerical simulation of the nonlinear behavior of RC beams strengthened with NSM CFRP strips", *CMNE/CILAMCE 2007*, Abstract pp. 289, Paper nº 485 published in CD – FEUP, 20 pp., Porto, 13, 13-15 June, 2007.

[6] Barros, J.A.O.; Pereira, E.B.; Santos, S.P.F., "Lightweight panels of steel fiber reinforced self-compacting concrete", *Journal of Materials in Civil Engineering*, 19(4), 295-304, 2007.

[7] Sena-Cruz, J.M., "Strengthening of concrete structures with near-surface mounted CFRP laminate strips.", *PhD Thesis*, Department of Civil Engineering, University of Minho, 2004, <http://www.civil.uminho.pt/composites>

[8] Hofstetter, G. and Mang, H. A., "Computational mechanics of reinforced concrete structures", *Friedr. Vieweg & Sohn Verlagsgesellschaft mbH*, Germany, 1995.

[9] Rots, J.G., "Computational modeling of concrete fracture", *Dissertation*, Delft University of Technology, 1988.

[10] Rots, J.G. and de Borst, R., "Analysis of mixed-mode fracture in concrete", *Journal of Engineering Mechanics*, ASCE, *113(11)*, pp. 1739-1758, 1987.

[11] Barros, J.A.O.; Pereira, E.N.B.; Ventura-Gouveia, A.; Azevedo, A.F.M., "Numerical simulation of thin steel fiber self-compacting concrete structures", *ACI 435/544 Fall 2007 Puerto Rico Session 1: Deflection and stiffness issues in FRC and thin structural elements (Structural Implications and Material Properties)*, in CD, 25 pages, October 2007.